Applied Physics Express

The Japan Society of Applied Physics

LETTERS

Model for large magnetoresistance effect in p–n junctions

To cite this article: Yang Cao *et al* 2018 *Appl. Phys. Express* **11** 061304

View the article online for updates and enhancements.

This content was downloaded from IP address 219.246.33.41 on 01/06/2018 at 11:45

Applied Physics Express **11**, 061304 (2018)
https://doi.org/10.7567/APEX.11.061304

Model for large magnetoresistance effect in p–n junctions

Yang Cao, Dezheng Yang*, Mingsu Si, Huigang Shi, and Desheng Xue*

Key Laboratory for Magnetism and Magnetic Materials of Ministry of Education, Lanzhou University, Lanzhou 730000, China

*E-mail: yangdzh@lzu.edu.cn; xueds@lzu.edu.cn

Received April 12, 2018; accepted May 11, 2018; published online June 1, 2018

We present a simple model based on the classic Shockley model to explain the magnetotransport in nonmagnetic p–n junctions. Under a magnetic field, the evaluation of the carrier to compensate Lorentz force establishes the necessary space-charge region distribution. The calculated current–voltage (*I*–*V*) characteristics under various magnetic fields demonstrate that the conventional nonmagnetic p–n junction can exhibit an extremely large magnetoresistance effect, which is even larger than that in magnetic materials. Because the large magnetoresistance effect that we discussed is based on the conventional p–n junction device, our model provides new insight into the development of semiconductor magnetoelectronics. © 2018 The Japan Society of Applied Physics

Large magnetoresistance (MR) effects in nonmagnetic semiconductor devices will provide modern electronics with more functionality and applications, which will have a profound impact on the existing and emerging semiconductor industry. In contrast to the negligible MR in nonmagnetic semiconductors,[1] recently, extremely large MR effects have been reported in doped Ag_2Se,[2,3] InSb,[4] WTe_2,[5] GaAs,[6] Ge,[7–9] and Si.[10–19] The MR ratio of these materials can be comparable to and even larger than those of magnetic materials over a large temperature range.

There are presently two proposed explanations for the large MR effect in nonmagnetic materials. One is a quantum theory of the MR effect.[20,21] When the individual quantum levels associated with the electron orbits are distinct, these effects become noticeable. However, this makes practical realization unique to a few semiconductors having tiny pockets of the Fermi surface with a small effective mass. The other explanation is the model of inhomogeneity conductors.[22–28] Such inhomogeneity could produce a large spatial fluctuation in the conductivity tensor. In this case, the obtained large MR effect is derived from the deformation of current paths, which causes an uncompensated Hall field to be involved in transverse MR.

According to the inhomogeneity MR mechanism, the conventional p–n junction device can also be considered as a perfect system to obtain a large MR effect.[29–32] This is because the p–n junction takes advantage of the bipolar (electron and hole) nature of transport in an inhomogeneously doped semiconductor. The opposite sign of the carrier mobility between the electron and the hole can increase the fluctuation of the carrier mobility, which effectively enhances the MR effect.[5] More importantly, the transport properties of the p–n junction are dominated by the intrinsic space-charge region (SCR). Experiments have shown that manipulating the SCR in the p–n junction by applying a magnetic field can significantly affect the transport behavior, which leads to a large MR effect.[29–31]

In this work, we propose a model to demonstrate the large MR effect of the p–n junction. We will show in detail how the intrinsic SCR of the p–n junction evolves under a magnetic field and how the SCR distribution further causes the large MR effect of the p–n junction. Because our model is only based on the conventional p–n junction structure, the large MR effect of the p–n junction should be universal and useful for future magnetoelectronics.

The basis of our model is a conventional p–n junction structure. In Fig. 1(a), the left side is a p-type semiconductor

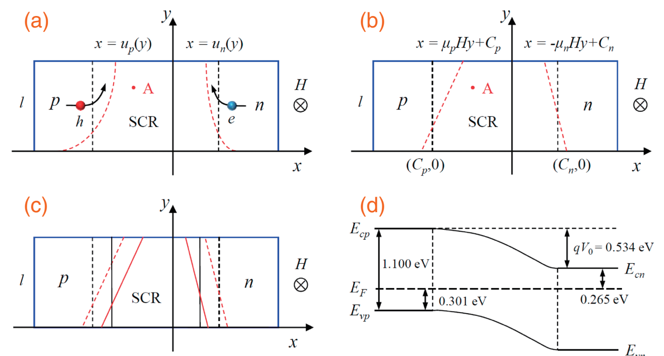

Fig. 1. Schematic illustration of the large MR effect in p–n junction originating as a result of the spatial distribution of the SCR induced by a magnetic field. (a) Without a magnetic field, the boundary of the SCR between p- and n-type semiconductors is uniform, as shown by the black dashed lines. However, when we apply an external magnetic field, the SCR will be redistributed, since the carriers in the p- and n-type regions are deflected by Lorentz force and accumulate at the edges of the junction. The redistribution boundaries of the SCR under the magnetic field are defined as $x = u_{p(n)}(y)$, and are represented as the red dashed lines. (b) According to our model, to balance the magnetic field, a trapezoidal distribution of the SCR with the slope $\mu_p H$ and $-\mu_n H$ is formed. The boundaries of the SCR under a magnetic field are represented by the red dashed lines. (c) The width of the SCR is adjusted by changing the external electric field; this is also known as the rectification effect of the p–n junction. When a forward voltage is applied, the SCR of the p–n junction shrinks from the dashed line to the solid line. The black line represents the rectification effect at zero magnetic field, and the red line represents the rectification effect under a magnetic field. (d) Calculated energy band diagram of silicon p–n junction at room temperature.

doped with N_a acceptors per unit volume, the right side is an n-type semiconductor with N_d donors per unit volume, and the middle region is the SCR. As we discussed above, it is the physics of the SCR that gives rise to the interesting electrical and magnetic properties of the bipolar p–n junction. When the width of the SCR is tuned by the electric field, the resistance of the p–n junction can vary by several orders of magnitude, i.e., from conducting to cut-off. This is also known as the rectification effect of the p–n junction. The following interesting question is what happens in the p–n junction under a magnetic field. Can the magnetic field also change the SCR, just like the electric field? In contrast to conventional semiconductors under a magnetic field, there are enough accumulated carriers to generate a Hall electric field to balance the Lorentz force. On the other hand, in the p–n junction, the mobilizable carriers in the SCR are too few

 © 2018 The Japan Society of Applied Physics

to balance the Lorentz force. Instead, a carrier concentration deviation is formed, which induces a diffusion process to compensate the Lorentz force in the SCR. This hypothesis is also confirmed by considering the carrier movement in the p- and n-type regions. The carriers in the p- and n-type regions are both deflected owing to the Lorentz force. The deflected carriers will accumulate at the boundary and thus change the SCR. As a result, the carrier concentration in the SCR shows a deviation.

To systematically analyze the evolution of the SCR under a magnetic field, we expand the classic Shockley model to describe the magnetic field effect. As shown in Fig. 1(a), without the magnetic field, the SCR is uniform. However, when the magnetic field is applied, the boundary of the SCR is tuned by the magnetic field and expressed as $x = u_p(y)$ and $x = u_n(y)$. Thus, the hole and electron current densities, $\boldsymbol{J}_p$ and $\boldsymbol{J}_n$, resulting from both the electric field $\boldsymbol{E}$ and the magnetic field $\boldsymbol{H}$, are shown as[33]

$$\boldsymbol{J}_p = q\mu_p p\boldsymbol{E} - qD_p\nabla p + q\mu_p p\boldsymbol{v}_p \times \boldsymbol{H}, \tag{1a}$$

$$\boldsymbol{J}_n = q\mu_n n\boldsymbol{E} + qD_n\nabla n - q\mu_n n\boldsymbol{v}_n \times \boldsymbol{H}, \tag{1b}$$

where q, p (n), μ_p (μ_n), D_p (D_n), and v_p (v_n) stand for carrier charge, concentration, mobility, diffusivity, and drift velocity for a hole (electron), respectively. The first term of Eq. (1) represents the drift of the carrier driven by an external electric field, the second term represents the diffusion of the carrier due to the concentration gradient, and the last term represents the carrier deflection due to Lorentz force under a magnetic field. When the p–n junction is in thermal equilibrium, the current density is zero, i.e., $\boldsymbol{J}_p = \boldsymbol{J}_n = 0$.

According to the electrostatic equation, the built-in electric field at an arbitrary position A(x, y) in Fig. 1(a) depends on the charge distribution, namely,

$$\nabla \cdot \boldsymbol{E}(x, y) = q(p(x, y) - n(x, y) + N_d - N_a)/\varepsilon, \tag{2}$$

where ε is the dielectric constant of silicon. Equation (2) is also known as Poisson's equation.

If we replace the drift velocity in Eq. (1) with

$$\boldsymbol{v}_p = \mu_p\boldsymbol{E}, \quad \boldsymbol{v}_n = -\mu_n\boldsymbol{E}, \tag{3}$$

we can solve the partial differential Eqs. (1a), (1b), and (2) to obtain the stable distributions of $\boldsymbol{E}(x, y)$, $p(x, y)$, and $n(x, y)$ under different magnetic fields H, by adding the appropriate boundary conditions.

To obtain an analytical solution, the above models are further simplified by the following assumptions. First, we assume that the magnetic field is along the z-direction. Second, we assume that the impurity ions in the SCR are all ionized, and the carriers entering the SCR are ignored. Thus, the amount of charge in the SCR is equal to the concentration of impurity ions implanted. Finally, we assume that the electric field in the SCR is only in the x-direction. Therefore, to consider the thermal equilibrium state of the p–n junction, the continuity Eq. (1a) for holes and Poisson's Eq. (2) can be rewritten as

$$q\mu_p p(x, y)E(x, y) - qD_p\frac{\partial p(x, y)}{\partial x} = 0, \tag{4}$$

$$-qD_p\frac{\partial p(x, y)}{\partial y} + q\mu_p p(x, y)[\mu_p E(x, y)]H = 0, \tag{5}$$

$$\nabla \cdot E(x, y) = -qN_a/\varepsilon. \tag{6}$$

Equation (4) describes that the carrier drift driven by the electric field is balanced by the carrier diffusion due to the carrier concentration deviation along the x-direction, while Eq. (5) describes that the carrier deflection driven by the magnetic field is balanced by the carrier diffusion due to the carrier concentration deviation along the y-direction. According to Eq. (6), we can obtain the distribution of the electric field, which depends on the boundary of the SCR,

$$E(x, y) = -qN_a(x - u_p(y))/\varepsilon. \tag{7}$$

When we substitute Eq. (7) into Eq. (4) and utilize Einstein's relation, we can obtain the distribution of the carrier concentration,

$$p(x, y) = p_p \exp\left[-\frac{q^2}{2kT\varepsilon}N_a(x - u_p(y))^2\right], \tag{8}$$

where p_p stands for the hole density in the p region ($p_p \approx N_a$), k is Boltzmann's constant, and T is temperature.

Finally, according to the continuity Eq. (5) along the y-direction, we can obtain the boundary of the SCR of the p region side using Eq. (8),

$$u_p(y) = \mu_p H_y + C_p. \tag{9}$$

Similarly, we can obtain the boundary of the SCR of the n region side,

$$u_n(y) = -\mu_n H_y + C_n. \tag{10}$$

According to Eqs. (9) and (10), one can easily find that the SCR under the magnetic field has a trapezoid distribution with the slopes $\mu_p H$ and $-\mu_n H$, as shown in Fig. 1(b). Thus, the width of the SCR (w) changes with y as $w = w_b - (\mu_p + \mu_n)H_y$, with $w_b = C_n - C_p$ being the bottom width of the SCR with the magnetic field, which leads to the injected minority carriers varying with y. We integrate and average the injected minority holes (electrons), $\overline{\Delta p_n}$($\overline{\Delta n_p}$), at the right (left) boundary of the SCR along the y-direction,

$$\overline{\Delta p_n} = N_a\left(\frac{\int_0^l \exp\left(-\frac{q}{\alpha kT}w^2\right)dy}{l} - \exp\left(-\frac{qV_0}{kT}\right)\right), \tag{11a}$$

$$\overline{\Delta n_p} = N_d\left(\frac{\int_0^l \exp\left(-\frac{q}{\alpha kT}w^2\right)dy}{l} - \exp\left(-\frac{qV_0}{kT}\right)\right), \tag{11b}$$

where $\alpha = (2\varepsilon/q) \cdot [(N_a + N_d)/N_a N_d]$, V_0 is the built-in potential difference of the p–n junction, and l is the length of the p–n junction along the y-direction, as shown in Fig. 1(b).

According to the Shockley theory, the current flow through the p–n junction is equal to the sum of the hole and electron diffusion currents, which are proportional to $\overline{\Delta p_n}$ and $\overline{\Delta n_p}$,[33]

$$I = \frac{qAD_p}{L_p}\overline{\Delta p_n} + \frac{qAD_n}{L_n}\overline{\Delta n_p}, \tag{12}$$

where A and L_p (L_n) stand for the cross-sectional area of the p–n junction and the diffusion length of holes (electrons), respectively. When we apply a voltage to the p–n junction, the boundary of the SCR under the magnetic field is correspondingly shifted to achieve a new balance to compensate

© 2018 The Japan Society of Applied Physics

the external electrical field. As shown in Fig. 1(c), the boundary of the SCR changes from the red dashed line to the red solid line when the forward voltage is applied. That is, the width of the SCR (w) in Eq. (11) changes to $w = w_b - (\mu_p + \mu_n)H_y - \alpha^{1/2}(V_0^{1/2} - (V_0 - V)^{1/2})$. Figure 1(d) shows the energy band diagram of our p–n junction at room temperature. The magnitude of the built-in potential difference V_0 is 0.534 V.

On the basis of the above model, we can calculate the current–voltage (*I*–*V*) curves under different magnetic fields at room temperature. The simulation parameters shown are close to the parameters of a real silicon-based p–n junction, where $N_a = 2.0 \times 10^{14}\,\text{cm}^{-3}$, $N_d = 1.0 \times 10^{15}\,\text{cm}^{-3}$, $\mu_p = 480\,\text{cm}^2\,\text{s}^{-1}\,\text{V}^{-1}$, and $\mu_n = 1350\,\text{cm}^2\,\text{s}^{-1}\,\text{V}^{-1}$. As shown in Fig. 2(a), all the *I*–*V* curves show the rectification effect. However, when the magnetic field is applied, the current is suppressed and gradually decreases as the magnetic field increases, indicating a large positive MR. Here, MR is defined as

$$\text{MR}\ (\%) = \frac{R(H) - R(0)}{R(0)}. \tag{13}$$

Notably, the calculated *I*–*V* curves under different magnetic fields are consistent with the experimental results.[29]

The corresponding MR curve at $V = 0.4$ V at various temperatures (T) is shown in Fig. 2(b). As the temperature increases, MR sharply decreases. For $H = 3.5$ T, at $T = 50$ K, MR can reach up to 4500%, while at $T = 300$ K, MR is about 2000%, which is even larger than those of the magnetic material devices. There are two features of the calculated MR. One is that, at a lower magnetic field, MR increases sharply. This indicates a higher magnetic sensitivity at the lower magnetic field. The other is that MR gradually shows linear magnetic field dependence when H is beyond 1.5 T, even up to 10 T. Notably, the calculated MR results are similar to the MR observed experimentally,[34] where a dynamic p–n junction is created by carrier injections from heavily doped n+ and p+ regions to the very lowly doped *n*-region. By utilizing the influence of the magnetic field on a dynamic p–n junction, the MR of the whole device can be amplified and a higher magnetic sensitivity is achieved at the lower magnetic field. We also calculate the MR in backward bias. For $H = 3.5$ T and $T = 300$ K, the MR is only 2% at $V = -0.1$ V, which is three orders of magnitude smaller than that at $V = 0.4$ V. This is consistent with our experimental results.

To optimize the MR effect of the p–n junction, we further adjust the doping concentration to obtain a large MR effect. We set $N_a N_d = 2 \times 10^{29}\,\text{cm}^{-3}$ to keep the built-in electrical potential V_0 unchanged. According to Caughey's empirical formulas for the mobility of silicon,[35] μ_n and μ_p as functions of N_d are depicted in Fig. 3(a). As N_d increases, the value of μ_n is almost unchanged for N_d up to $2 \times 10^{14}\,\text{cm}^{-3}$ and then drops sharply, while μ_p increases at the beginning and becomes saturated for $N_d > 2 \times 10^{15}\,\text{cm}^{-3}$. The N_d dependences of MR for various magnetic fields are calculated by substituting the above mobilities into our model. The inset in Fig. 3(b) shows the non-normalized MR as a function of N_d. Clearly, the larger MR is achieved at the higher magnetic field. However, we find that the normalized MR ratios for different magnetic fields exhibit the same behaviors, as shown in Fig. 3(b). The maximum MR occurs at $N_d = 3 \times 10^{14}\,\text{cm}^{-3}$. At this point, $N_d \approx N_a$, and the total mobility $\mu_t = \mu_n + \mu_p$ is also maximal. The maximum μ_t enhances the magnetic field influence of the SCR, thus resulting in the largest MR. Therefore, according to our calculation, N_a in the p region should be designed to equal N_d in the *n* region to obtain the maximal MR for the p–n junction. The lower (higher) donor impurity doping N_d will

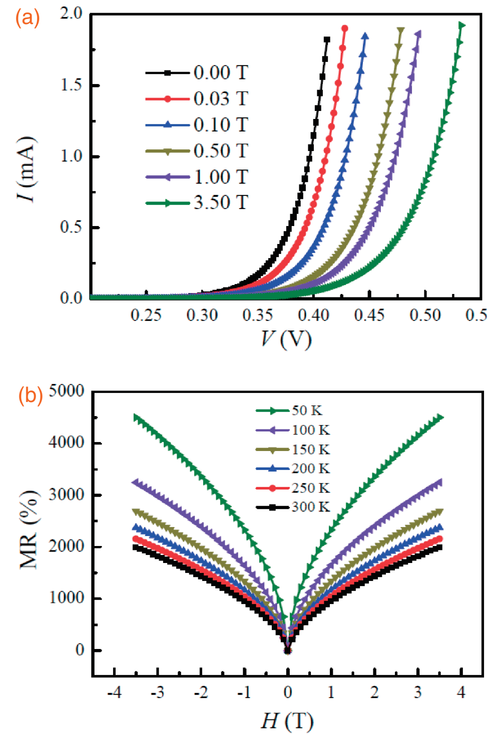

Fig. 2. (a) Calculated *I*–*V* curves of the p–n junction at room temperature for various magnetic fields. From left to right, the magnetic field is increased from 0 to 3.5 T. (b) Calculated MR curves of the p–n junction at a fixed voltage $V = 0.4$ V at different temperatures. From top to bottom, the temperature is increased from 50 to 300 K.

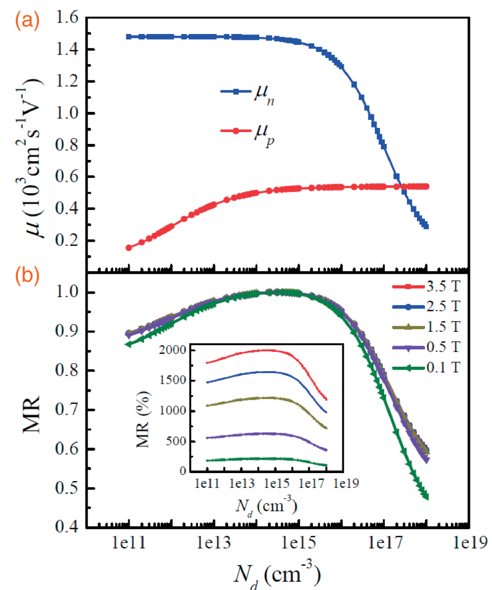

Fig. 3. (a) Electron (hole) mobility μ_n (μ_p) as a function of the donor doping concentration N_d, obtained using Caughey's empirical formulas. Here, we set $N_a N_d = 2 \times 10^{29}\,\text{cm}^{-3}$ to keep the built-in electrical potential V_0 unchanged. (b) Normalized MR as a function of N_d for various magnetic fields. The inset shows the non-normalized MR as a function of N_d for various magnetic fields.

© 2018 The Japan Society of Applied Physics

reduce the hole (electron) mobility because of the ionized impurity scattering, which induces the decrease in μ_t.

In summary, we proposed a simple model to explain the large MR effect discovered experimentally in the silicon-based p–n junction. In contrast to conventional semiconductors, where the electric field due to the accumulated carriers is formed to balance the Lorentz force, owing to the variation of the SCR in the p–n junction, a concentration gradient is formed, which leads to a diffusion process to balance the Lorentz force. The analysis further showed that the SCR has a trapezoidal distribution under a magnetic field, and the slopes of the two sides are related to μH. The calculated I–V characteristics and MR characteristics of the p–n junction are consistent with the experimental results, proving the accuracy of the model. Moreover, we suggest that the MR of the p–n junction can be enhanced by both enhancing the mobility and modulating the donor concentration to equal the acceptor concentration. Our computer simulation results reveal the origin of MR in the p–n junction and indicate a viable avenue for magnetoelectric devices based on semiconductors.

Acknowledgments This work is supported by the NSFC of China (Grant Nos. 11774139, 51372107, and 11674143), PCSIRT (Grant No. IRT-16R35), and the Program for Science and Technology of Gansu Province (Grant No. 17YF1GA024).

1) A. Sommerfeld and H. N. Frank, Rev. Mod. Phys. **3**, 1 (1931).
2) R. Xu, A. Husmann, T. F. Rosenbaum, M.-L. Saboungi, J. E. Enderby, and P. B. Littlewood, Nature **390**, 57 (1997).
3) J. S. Hu, T. F. Rosenbaum, and J. B. Betts, Phys. Rev. Lett. **95**, 186603 (2005).
4) S. A. Solin, T. Thio, D. R. Hines, and J. J. Heremans, Science **289**, 1530 (2000).
5) M. N. Ali, J. Xiong, S. Flynn, J. Tao, Q. D. Gibson, L. M. Schoop, T. Liang, N. Haldolaarachchige, M. Hirschberger, N. P. Ong, and R. J. Cava, Nature **514**, 205 (2014).
6) Z. G. Sun, M. Mizuguchi, T. Manago, and H. Akinaga, Appl. Phys. Lett. **85**, 5643 (2004).
7) J. J. Chen, X. Z. Zhang, Z. C. Luo, J. M. Wang, and H. G. Piao, J. Appl. Phys. **116**, 114511 (2014).
8) B. Cheng, H. W. Qin, and J. F. Hu, J. Phys. D **50**, 445001 (2017).
9) K. Zhang, H. H. Li, P. Grünberg, Q. Li, S. T. Ye, Y. F. Tian, S. S. Yan, Z. J. Lin, S. S. Kang, Y. X. Chen, G. L. Liu, and L. M. Mei, Sci. Rep. **5**, 14249 (2015).
10) J. J. H. M. Schoonus, F. L. Bloom, W. Wagemans, H. J. M. Swagten, and B. Koopmans, Phys. Rev. Lett. **100**, 127202 (2008).
11) J. J. H. M. Schoonus, P. P. J. Haazen, H. J. M. Swagten, and B. Koopmans, J. Phys. D **42**, 185011 (2009).
12) M. P. Delmo, S. Kasai, K. Kobayashi, and T. Ono, Appl. Phys. Lett. **95**, 132106 (2009).
13) M. P. Delmo, S. Yamamoto, S. Kasai, T. Ono, and K. Kobayashi, Nature **457**, 1112 (2009).
14) M. P. Delmo, E. Shikoh, T. Shinjo, and M. Shiraishi, Phys. Rev. B **87**, 245301 (2013).
15) N. A. Porter and C. H. Marrows, J. Appl. Phys. **109**, 07C703 (2011).
16) N. A. Porter and C. H. Marrows, Sci. Rep. **2**, 565 (2012).
17) C. H. Wan, X. Z. Zhang, X. L. Gao, J. M. Wang, and X. Y. Tan, Nature **477**, 304 (2011).
18) L. H. Wu, X. Zhang, J. Vanacken, N. Schildermans, C. H. Wan, and V. V. Moshchalkov, Appl. Phys. Lett. **98**, 112113 (2011).
19) C. H. Wan, Z. H. Yuan, P. Liu, H. Wu, P. Guo, D. L. Li, and S. S. Ali, Appl. Phys. Lett. **103**, 262406 (2013).
20) A. A. Abrikosov, Phys. Rev. B **58**, 2788 (1998).
21) A. A. Abrikosov, Europhys. Lett. **49**, 789 (2000).
22) M. M. Parish and P. B. Littlewood, Nature **426**, 162 (2003).
23) M. M. Parish and P. B. Littlewood, Phys. Rev. B **72**, 094417 (2005).
24) J. Hu, M. M. Parish, and T. F. Rosenbaum, Phys. Rev. B **75**, 214203 (2007).
25) D. Stroud and D. J. Bergman, Phys. Rev. B **30**, 447 (1984).
26) V. Guttal and D. Stroud, Phys. Rev. B **71**, 201304 (2005).
27) R. Magier and D. J. Bergman, Phys. Rev. B **74**, 094423 (2006).
28) A. Shik, *Electronic Properties of Inhomogeneous Semiconductors* (Gordon and Breach, Philadelphia, PA, 1995).
29) D. Z. Yang, F. C. Wang, Y. Ren, Y. L. Zuo, Y. Peng, S. M. Zhou, and D. S. Xue, Adv. Funct. Mater. **23**, 2918 (2013).
30) T. Wang, M. S. Si, D. Z. Yang, Z. Shi, F. C. Wang, Z. L. Yang, S. M. Zhou, and D. S. Xue, Nanoscale **6**, 3978 (2014).
31) D. Z. Yang, T. Wang, W. B. Sui, M. S. Si, D. W. Guo, Z. Shi, F. C. Wang, and D. S. Xue, Sci. Rep. **5**, 11096 (2015).
32) F. Chiodi, S. L. Bayliss, L. Barast, D. Débarre, H. Bouchiat, R. H. Friend, and A. D. Chepelianskii, Nat. Commun. **9**, 398 (2018).
33) B. G. Streetman and S. K. Banerjee, *Solid State Electronic Devices* (Prentice-Hall, Upper Saddle River, NJ, 2006).
34) T. Wang, D. Z. Yang, M. S. Si, F. C. Wang, S. M. Zhou, and D. S. Xue, Adv. Electron. Mater. **2**, 1600174 (2016).
35) S. Adachi, *Properties of Group-IV, III–V and II–VI Semiconductors* (Wiley, New York, 2005).

© 2018 The Japan Society of Applied Physics